Distribution of point defects in Si(100)/Si grown by low-temperature molecular-beam epitaxy and solid-phase epitaxy

P. Asoka-Kumar
Department of Physics, Brookhaven National Laboratory, Upton, New York 11973

H.-J. Gossmann, F. C. Unterwald, and L. C. Feldman
AT&T Bell Laboratories, 600 Mountain Avenue, Murray Hill, New Jersey 07974

T.C. Leung, H.L. Au, V. Talyanski, B. Nielsen, and K.G. Lynn
Department of Physics, Brookhaven National Laboratory, Upton, New York 11973
(Received 27 January 1993)

Positron annihilation in Si is a quantitative, depth-sensitive technique for the detection of vacancy-like defects or voids. A sensitivity of 5×10^{15} cm^{-3} for voidlike defects is easily achieved. The technique has been applied to a study of point-defect distributions in thin films of Si grown by molecular-beam epitaxy. A special procedure was developed to remove the influence of the native oxide on the positron measurement. 200-nm-thick films grown at temperatures between 475 and 560 °C show no defects below the sensitivity limit and are indistinguishable from the bulk substrate. So are films grown at 220 °C, provided a 2-min high-temperature anneal to a peak temperature of $\geq$ 500 °C is executed every $\simeq$ 30 nm during growth. If $T_{\mathrm{RTA}} = 450$ °C, part of the film contains vacancylike defects to a concentration of $\simeq 10^{18}$ cm^{-3}. These results correlate well with current-voltage characteristics of *p-n* junctions grown with different rapid thermal anneal (RTA) temperatures. Ion scattering, with a defect sensitivity of $\approx 1\%$, shows no difference between films grown with different T_{RTA}. Recrystallization of amorphous films, deposited at room temperature and annealed *in situ* at 550 °C, always leaves a significant defect concentration of $\simeq 2 \times 10^{18}$ cm^{-3}; those defects are reduced but still present even after a 2-h, 800 °C furnace anneal.

I. INTRODUCTION

The growth and doping of thin films by molecular-beam epitaxy (MBE) allows the engineering of composition and doping profiles, leading to the realization of novel device concepts and physical phenomena. However, the capabilities of MBE can only be exploited fully if segregation and diffusion can be suppressed sufficiently. Indeed this has placed significant restrictions on Si MBE from the beginning[1] since at the typical growth temperatures of $\gtrsim$ 400 °C for Si, incorporation of dopants is dominated by severe surface segregation.[2] Recently, it was shown that the concept of an epitaxial *temperature*, T_{epi}, separating the regime of crystalline and epitaxial growth of silicon, is not appropriate and should be replaced with the concept of a limiting epitaxial *thickness* h_{epi} that has an exponential dependence on the growth temperature.[3] Epitaxy in excess of h_{epi} is achieved by interrupting the growth with short annealing cycles [rapid thermal anneal (RTA)] before reaching h_{epi}, typically of a duration $\sim$ 2 min, with a peak temperature of $\simeq$ 500 °C.[3,4] This allows crystalline growth at arbitrary temperatures in a regime where segregation and diffusion is completely suppressed kinetically (low-temperature MBE, LT-MBE). Typical growth temperatures are of the order of 250 °C. Excellent control over the incorporation of dopants is achieved in films grown by low-temperature Si MBE, without any post-growth annealing.[5,6]

The very low growth temperature employed in LT-MBE raises the question as to the existence of point defects, such as vacancies, in the film. Conventional techniques (electron microscopy, ion scattering) show the absence of extended defects, and place a relatively high limit on point-defect concentrations. Positron annihilation spectroscopy (PAS), on the other hand, is uniquely suited for the detection of low concentrations ($\gtrsim 10^{-7}$ atomic concentration) of open-volume-type defects in crystalline solids.[7] Here we examine the defect distributions in films grown by LT-MBE using variable energy positrons and compare these results with ion-scattering and electrical measurements. We show that under appropriate growth conditions Si films grown at temperatures as low as 220 °C are indistinguishable from bulk materials as viewed by positrons. On the other hand, films grown by solid-phase epitaxy (SPE), i.e., a deposition of amorphous film followed by *in situ* regrowth, contain a substantial amount of vacancylike defects, even after high-temperature annealing.

II. BACKGROUND

Positrons implanted into a solid penetrate to a mean depth determined by the incident beam energy.[8] During this step, positrons lose their kinetic energy through a multitude of collisions and attain thermal energies.

The thermalized positrons diffuse and annihilate with electrons, either from a freely diffusing state or from a trapped state (at a defect site), predominantly producing two 511-keV γ rays. Because the positrons are thermalized, the Doppler broadening of these annihilation γ rays is dominated by the electron momentum distribution around the annihilation site and can be used to distinguish annihilations originating from a perfect crystal and from a crystal with various kinds of open-volume-type defects.

The Doppler broadening of the annihilation γ rays can be quantified by a shape parameter S, defined as the ratio between the counts appearing in a small region of fixed energy width ($\sim$ 1.59 keV) around the center energy of 511 keV and the total number of counts in the annihilation photopeak. Lower electron momenta around the annihilation site will produce a sharper annihilation spectrum and hence a higher S value, and vice versa. Previous studies have established a high-S value for annihilations from defect sites or vacancies, where the localized positrons are less likely to encounter the high-momentum core electrons.[9,7]

The S parameter is usually measured as a function of positron beam energy E, resulting in a S-E curve as described below. The S-E values are analyzed using a one-dimensional, steady-state, diffusion-annihilation equation along with the initial condition of a derivative-Gaussian implantation profile for positrons.[7] The positron volume density $n(z)$ is determined by

$$D_+ \frac{d^2n(z)}{dz^2} - \frac{d[v_d(z)n(z)]}{dz} - [k_t c(z) + \lambda_b]n(z) + I(z,E) = 0\,, \quad (1)$$

where z is the depth measured into the film from the surface, D_+ is the positron diffusion coefficient, $v_d(z)$ is the field-dependent drift velocity, k_t is the specific trapping rate in defects, $c(z)$ is the depth-dependent concentration of defects (in units of atomic fraction), and λ_b is the bulk annihilation rate. The positron diffusion coefficient D_+ is related to the positron diffusion length in defect-free silicon by $L_+ = (D_+/\lambda_b)^{1/2}$. $I(z,E)$ is the positron stopping rate (density increase/sec), and is proportional to the first derivative of a Gaussian[7]

$$I(z,E) \propto \frac{d}{dz}\exp[-(z/z_0)^2], \quad (2)$$

where z_0 is an energy-dependent parameter related to the mean implantation depth $\bar{z}$ by $z_0 = 2\bar{z}/\sqrt{\pi}$. The mean implantation depth (in units of Å) is given by

$$\bar{z} = \frac{400}{\rho}E^{1.6}\,, \quad (3)$$

where ρ is the density of the material in g/cm^3 and E is in keV.

The above diffusion-annihilation equation is solved to determine the fraction of positrons T_i, annihilating in each region of a multilayered structure. The S parameter as a function of positron energy E is then given by

$$S(E) = \sum_i^N S_i T_i\,, \quad (4)$$

where S_i is the S parameter for the ith layer and N is the total number of layers. A best fit of Eq. (4) to experimental data is then obtained with the aid of a program VEPFIT (Ref. 10), by varying S_i and diffusion lengths. For data collected at room temperature the electric fields also are treated as free parameters. When studying an unknown layer structure, such as a system with an unknown defective layer, boundaries between the layers also can be varied.

The positron trapping at defect sites is related to the effective diffusion length modified by the presence of defects $L_{+,\mathrm{eff}}$ by

$$k_t c(z) = \left[\left(\frac{L_+}{L_{+,\mathrm{eff}}(z)}\right)^2 - 1\right]\lambda_b\,. \quad (5)$$

The annihilation rate of positrons in defect-free silicon is $\lambda_b = 4.5 \times 10^9$/s.[11] The specific trapping rates for vacancylike defects in Si are $\sim 10^{15}$ s^{-1}.[12] The Doppler-broadening measurements alone cannot distinguish between various kinds of point defects. As we will show below the measured S parameter for those layers where defects are present is indicative of vacancylike defects, divacancies, or larger.[13] The present S-parameter measurement is unable to distinguish uniquely between various vacancylike defects. However, the specific trapping rate is not dependent sensitively on the exact assignemnt; we will use a specific trapping rate of 10^{15} s^{-1} in the analysis. The bulk diffusion length L_+ is obtained by fitting the S-E data of a Si control sample similar to the one used as the substrate for the MBE growth. Commercially available substrates are defect free from the positron point of view.

III. EXPERIMENT

The samples were grown in a custom MBE system of base pressure 4×10^{-11} torr. Si was evaporated at rates of 0.02 nm/s from an e-beam evaporator. Si(100) substrates, of nominally zero miscut, were chemically cleaned and a protective oxide layer was grown as the final step.[14] Substrates were p doped with boron to a resistivity of 1000 Ω cm. The oxide was thermally desorbed *in situ* by the Si-beam cleaning technique[15] at a temperature of 800 °C and a Si deposition rate of 1.6×10^{13} cm^{-2} s^{-1} for a total of 1.5 nm. A Si buffer layer was subsequently grown of thickness $\approx$ 20 nm at temperature between 250 °C and 850 °C. Subsequently the actual films were grown at temperatures between 220 °C and 560 °C. At $T_{\mathrm{growth}} = 220$ °C the epitaxial thickness is $\approx$ 100 nm. To prevent the film from becoming amorphous 2-min RTA cycles were performed to a peak temperature T_{RTA} every $\approx$ 30 nm (Fig. 1). Deposition was also carried out at room temperature without RTA cycles. There $h_{\mathrm{epi}} \leq 5$ nm and the essentially amorphous films were recrystalized *in situ* at a temperature of 550°C [solid-phase epitaxy, (SPE)]. The completion of the regrowth was monitored by reflection high-energy electron diffrac-

tion (RHEED). The growth specifications of the samples are summarized in Table I.

The accurate determination of the wafer temperature in a MBE system is a difficult task. The conventional approaches of temperature measurement in ultrahigh vacuum, infrared pyrometry, and thermocouple measurements cannot be used in the temperature regime of interest under the restrictions of an ultraclean environment. However, wafer temperatures, even below 0 °C, can be accurately determined by laser interferometry.[16] In this method, the interference fringes produced by laser light reflected from the front and back side of a double-sided, polished wafer are counted as a function of wafer temperature. In our experimental geometry, using 1.52-μm laser light, a 2π phase shift corresponds to a temperature difference of 5 K, so that in principle a precision of 1 K is achievable. The actual accuracy in temperature measurement is essentially determined by the error in the measurement of the wafer thickness, about ± 2 μm, which corresponds to ± 2 °C at 550 °C. This technique requires a double-sided polished wafer, which is not practical for the actual device growth due to restrictions imposed by subsequent processing equipment. All films were thus grown on single-sided, polished wafers at certain settings of the heater power. The heater power in turn was calibrated in terms of temperature using a 20-Ω cm p-doped doubly polished wafer. The backsides of the regular samples and the calibration wafer differ in emissivity, i.e., for a given temperature the heater power will be higher for the double-sided polished wafer. This effect was corrected for by determining the additional heater power required to bring the calibration wafer to the same temperature, as measured by the pyrometer, as the regular samples, for temperatures around 500 °C. With this correction, the power program used for the regular wafers was then executed on the calibration wafer and the temperature determined by laser interferometry. An example is shown in Fig. 1.

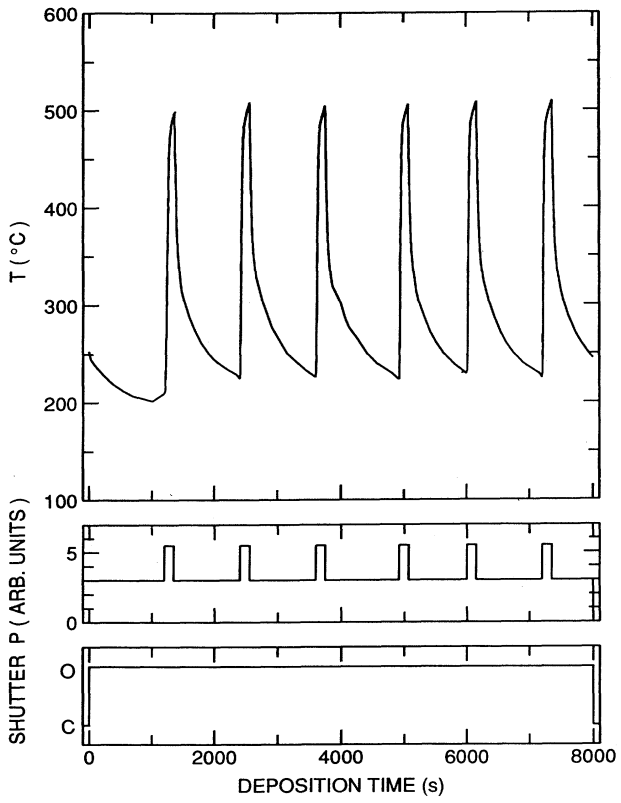

FIG. 1. Wafer temperature as a function of time during MBE growth at a growth temperature T_{growth} = 220 °C with 2.5-min flashes to 500 °C. The heater power P is indicated. No growth interruption took place during rapid thermal anneals, i.e. the shutter stayed open (O) all the time.

TABLE I. The growth specifications of samples used in the present study. The Si(100) substrate is B doped with a nominal resistivity of 1000 Ω cm; t_{film} denotes the film thickness, T_{growth} the growth temperature, and T_{RTA} the peak temperature reached during the rapid thermal anneal cycle. Rapid thermal anneals of 2-min duration were executed every ≈ 30 nm without growth interruptions. The SPE film was deposited at room temperature (RT) and was regrown at 550 °C.

t_{film} (nm)	T_{growth} (°C)	T_{RTA} (°C)
200	560	–
200	475	–
200	220	600
200	220	500
200	220	450
300	220	450
200	RT	–

The true temperature profile of the wafer during the growth process is thus known with the following assumptions. (1) The emissivity of the polished back side of a 20-Ω cm wafer agrees with that of a 1000-Ω cm wafer of the same dopant type to within ± 3% (this would result in a temperature error of ≃ ±10 °C). This assumption is needed to correct for the heater power between the single- and double-sided polished wafer. (2) Thermal conductivity through the wafer clamps and the heater block to the chamber environment is always the same. Experience shows that assumption (2) is true to better than ± 20 °C. We therefore estimate that the temperature scale is known to within an accuracy of ±20 °C.

The surface of the MBE Si film was chemically prepared prior to positron analysis. A bare silicon surface exposed to ambient will grow a *native* oxide layer of 1–2-nm thickness.[17] In addition to the native oxide, the surface may also contain other contaminants like sodium. To achieve a reproducible surface condition, the native oxide layer was etched away in a solution of ~ 1 part of 48% HF to 20 parts of distilled water for 10 sec followed by a dip in distilled water for another 10 sec. The process was repeated three times for all samples. Besides the removal of the oxide, HF cleaning results in a chemically stable Si surface.[18–20] After cleaning, it took about 55 min to transport and mount the sample into the positron analysis chamber and pump down the system into the high 10^{-6}-torr region. During this time the sample was ex-

posed to air directly for a total of $\sim$ 15 min. The base pressure during the data acquisition ranged from low to high 10^{-8} torr.

A variable energy positron beam (0–25 keV, in steps of 0.25 keV) was used for the measurements. The details of the experimental setup can be found elsewhere.[21] The positron beam intensity during the measurement was $\sim 5\times10^5$ e^+/s, too low to produce any measurable radiation damage during the experiment. The annihilation γ rays were detected with a cooled Ge detector.

The data were collected for one sample at a time. Before the cleaning process, an *S-E* scan at room temperature was carried out for each of the samples and this first *S-E* scan served as a measure of the effectiveness of the HF etching process. After the cleaning, the room-temperature *S-E* scan was repeated and was followed by the sequence: $T_m = T_a = 20\,^\circ$C, $T_m = T_a = 200\,^\circ$C, $T_m = 20\,^\circ$C and $T_a = 200\,^\circ$C, $T_m = T_a = 350$–$400\,^\circ$C, and $T_m = 20\,^\circ$C and $T_a = 350$–$400\,^\circ$C, where T_m is the sample temperature during the measurement and T_a is the heat-treatment temperature. The heat treatment (anneal) lasted for 10 h. The sample temperature in the positron chamber was maintained by a resistively heated tantalum foil which also held the sample. The temperature was monitored by a type-*K* thermocouple, calibrated prior to the measurement with a single-color infrared pyrometer[22] at temperatures $> 500\,^\circ$C. The temperature of the sample during the positron measurement was estimated to be within $\pm$ 25 °C of the measured value. A typical data collection time for each data point in an *S-E* scan was $\sim$ 4 min for 10^6 counts in the annihilation photopeak.

IV. RESULTS AND DISCUSSION

A. Defects in films grown by LT-MBE

The results of the *S-E* scan for the control Si sample, high-temperature MBE-grown sample, and a 220 °C MBE-grown sample are shown in Fig. 2. For each of the samples the plot shows room-temperature measurements before and after wet HF removal of native oxide film from the surface. The comparison of the curves brings out the following features. After the HF cleaning, the *S* parameter at the surface (low-incident energy) approaches the *S* parameter for the silicon bulk ($>$ 15 keV). The lower surface *S* parameter prior to HF treatment is an artifact due to a native thin oxide layer. Previous results on a thermally grown SiO_2-Si(100) system have shown that the *S* parameter for SiO_2 is lower than bulk silicon.[23] Because the native oxide layer has a different *S* value compared to the HF etched Si surface, the slope of the *S-E* data near the surface can be used to determine the positron diffusion length in bulk silicon. The fitted result is $L_+ = 200$ nm, in agreement with previous studies,[24] and is used as a fixed parameter for the diffusion length of positrons in defect-free silicon.

In addition, the measurements show that the MBE samples grown at temperatures as low as $T_{\rm growth} = 220\,^\circ$C with periodic rapid thermal anneal at $T_{\rm RTA} = 600\,^\circ$C is as good as the control sample and films grown at high temperatures. The *S* parameter values for the epitaxial layers are the same as the substrate wafer and are indistinguishable from the *S* values for the control wafer after HF cleaning.

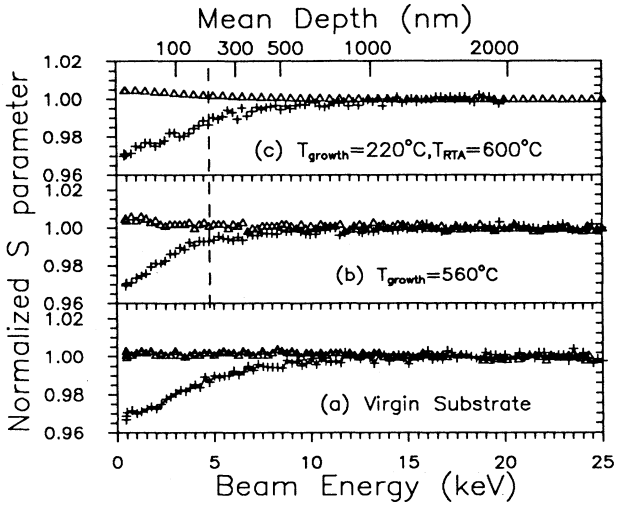

FIG. 2. *S* parameter vs energy curves for control silicon and MBE-grown Si/Si before (+) and after ($\triangle$) the removal of the native oxide layer by a dilute HF etch. The results are from (a) a virgin Si(100) substrate (control), (b) 200 nm of Si grown at $T_{\rm growth} = 560\,^\circ$C, and (c) 200 nm of Si grown at $T_{\rm growth} = 220\,^\circ$C with $T_{\rm RTA} = 600\,^\circ$C. The surface *S* parameter for the bulk silicon and clean silicon surface with hydrogen termination are similar. The broken line in panels (b) and (c) indicates the estimated epilayer-substrate boundary. All measurements are performed at room temperature ($\sim 20\,^\circ$C).

Figure 3 shows the *S-E* results from the low-temperature MBE samples that are subjected to different RTA temperatures. In all cases shown in Fig. 3, the MBE films were 200 nm thick. A sharp transition in the defect concentration of the film is observed when the RTA temperature is lowered below 500 °C. The *S* parameter near the surface region of the sample with $T_{\rm RTA} = 450\,^\circ$C is larger than the value for bulk silicon, indicating the presence of open volume defects. Note that cross-sectional TEM of samples grown under identical conditions shows no defects of any kind. The observed increase in *S* for $T_{\rm RTA} = 450\,^\circ$C is indicative of vacancy-like defects (divacancies or larger).[13] A similar high *S* parameter value is observed in a 300-nm-thick MBE layer grown with $T_{\rm RTA} = 450\,^\circ$C. The solid curves through the data points are obtained from the model and are discussed below.

Figure 4 shows the comparison of the *S-E* measurements at elevated temperatures (200 °C and 350–440 °C) to room-temperature measurements of high-temperature MBE grown- and control Si samples. The S-E curves were all measured after stabilizing the system at the elevated temperatures. This was verified by repeated *S-E* scans at elevated temperatures. The *S-E* values measured at room temperature after the 200 °C anneal were identical to the 20 °C measurement prior to the start of the annealing series for all the samples. This confirms that the defects are not structurally transformed under a prolonged 200 °C anneal. However, the samples which

were not subjected to the HF etch changed after the 200 °C anneal.

The 200 °C and the room-temperature measurement can differ mainly due to the electric field, which may be present at room temperature but disappears at 200 °C by the influence of thermally activated charge carriers. For all samples shown in Fig. 4, the 200 °C and 20 °C measurements were similar, indicating the absence of any electric field. Hence, we can rule out the possibility of an electric field hindering the diffusion of the positrons towards the surface. Thus, the S value of a HF-treated surface is similar to bulk Si, the exact cause of which is not understood. The surface S value for MBE-grown Si (both conventional high temperature and the low temperature grown) show a different behavior from control silicon. The surface S value at 200 °C is lower than at 20 °C for control Si, whereas the reverse is true for MBE silicon. The reason for this difference is not understood. The increase of the surface S value at 350–440 °C is due to the formation of positronium at the surface.[7]

The S-E measurements of the defective sample at elevated temperatures show electric-field effects. In Fig. 5 results for a sample with T_{growth} = 220 °C, T_{RTA} = 450 °C are shown. The 200 °C S-E curve differs from the 20 °C curve due to the electric field arising from the charged defect centers in the MBE-grown layer. A simi-

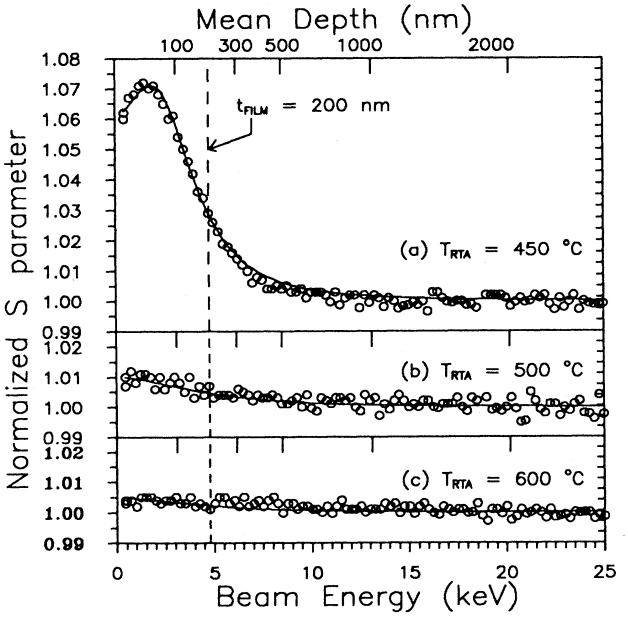

FIG. 3. A direct comparison between MBE samples grown at 220 °C, but with different rapid thermal anneal temperatures. The data correspond to T_{RTA} of (a) 450, (b) 500, and (c) 600 °C. The measurements were taken at room temperature after HF removal of the native oxide layer from the surface. The solid lines through the data points are the fitted curves. The data demonstrate that a rapid thermal anneal $\geq$ 500 °C is required to produce epitaxial layers that are thicker than the limiting epitaxial thickness, h_{epi}. The dashed line indicates the epilayer-substrate boundary estimated from a power law, $\bar{z} = \frac{400}{\rho}E^{1.6}$, where $\bar{z}$ is the mean depth, ρ is the density of the material, and E is the incident positron energy.

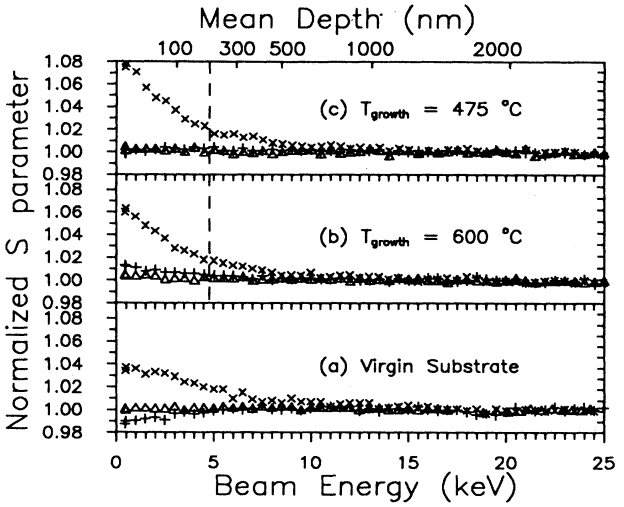

FIG. 4. S parameter vs energy curves at various analysis temperatures for control silicon and high-temperature-grown MBE silicon. The data correspond to (a) a virgin Si(100) substrate (control), (b) 200 nm of Si grown with T_{growth} = 600 °C, and (c) 200 nm of Si grown with T_{growth} = 475 °C. The symbols denote (△) $T_m = T_a$ = 20 °C, (+) $T_m = T_a$ = 200 °C, and (×) $T_m = T_a$ = 400–440 °C. The 200 °C measurement and 20 °C measurement are comparable and indicate the absence of trapped charges in the epilayer. The dashed line indicates the epilayer-substrate boundary estimated with a power law, $\bar{z} = \frac{400}{\rho}E^{1.6}$, where $\bar{z}$ is the mean depth, ρ is the density of the material, and E is the incident positron energy.

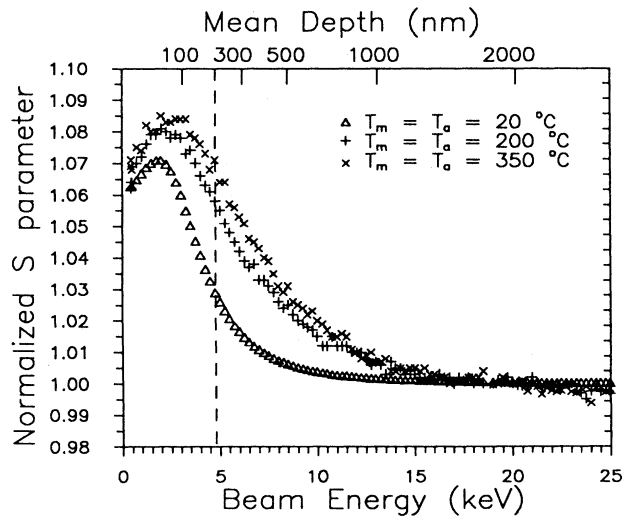

FIG. 5. S parameter vs energy curves for 200 nm of Si film grown on Si(100) at T_{growth} = 220 °C with T_{RTA} = 450 °C. The dashed line indicates the nominal epilayer-substrate boundary. The symbols denote: (△) $T_m = T_a$ = 20 °C, (+) $T_m = T_a$ = 200 °C, and (×) $T_m = T_a$ = 350 °C. The 200 °C measurement is different from the 20 °C measurement due to the absence of the electric field.

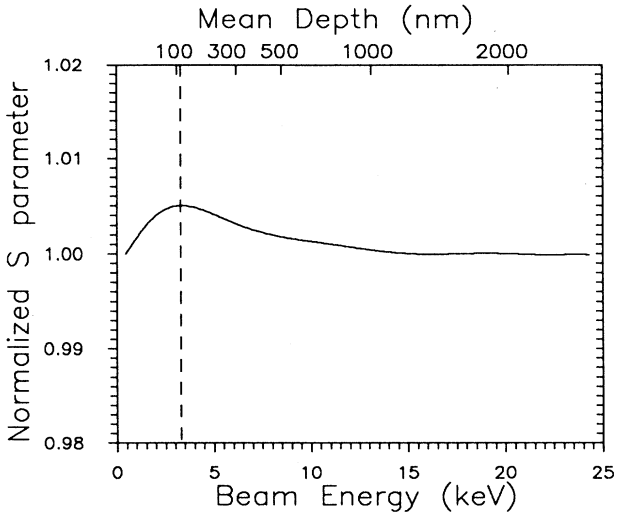

FIG. 6. A simulated S parameter vs energy curve illustrating the sensitivity of the technique to divacancylike defects. The curve was generated with a 120-nm-thick defective layer with a concentration of 5×10^{15} cm^{-3}. The defective layer S parameter was chosen as $1.03S_b$, where S_b corresponds to bulk silicon S value. The modeling is performed with the VEPFIT program.

lar trend is observed for a sample grown under identical conditions, but with a 300-nm MBE layer. The 350 °C anneal resulted in permanent changes of the defects so that the 20 °C measurement before the annealing cycle cannot be reproduced.

The results from the defective samples were further analyzed to obtain the defect-layer boundary, defect concentration, and electric field by the method outlined in Sec. II. For $T_{\mathrm{RTA}} \geq 500$ °C the S-E curves are similar to the control sample. Hence no further analysis was done for these measurements and an upper limit of 5×10^{15} cm^{-3} can be set for the defect concentration assuming a trapping rate of 10^{15} sec^{-1}.

This sensitivity limit of 5×10^{15} cm^{-3} is obtained by generating data with VEPFIT. This is illustrated in Fig. 6, where a model S-E curve generated with a defect concentration of 5×10^{15} cm^{-3} is shown. In generating the model curve, we assumed a 120-nm-thick defective layer, which is a typical thickness in our case. The S parameter for the defective layer is assumed to be $1.03S_b$, a lower limit for the S parameter of a layer with divacancies. The surface S value used is the same as for bulk silicon. A higher S value for the surface will decrease the sensitivity limit even further. It is clear from Fig. 6 that a concentration of 5×10^{15} cm^{-3} should be easily observable and that this sensitivity limit is quite conservative.

A two-layer model, comprising a top defective layer and an underlying defect-free silicon layer, was sufficient to fit the S-E data of samples with $T_{\mathrm{RTA}} = 450$ °C. We do not include the substrate as a separate layer, which is always assumed to be defect free. The free parameters used in the fitting are the defective layer thickness, the effective diffusion length, and the electric field. Because the diffusion length within a layer is held constant in the VEPFIT program, the defect concentration derived from Eq. (5) is uniform within a layer. The fitted results are summarized in Table II. The electric field is directed into the substrate silicon for the 20 °C measurements. For elevated temperature measurements, a satisfactory fit was obtained without introducing an electric field. The fitted boundary of the defective layers are $\sim$ 120 nm and $\sim$ 170 nm from the surface, respectively. Since these samples have a 200- and 300-nm epilayer, the first 80 and 130 nm of silicon films in the growth direction are bulk like, with an upper limit of 5×10^{15} cm^{-3} on defect concentrations. The observation of a nondefected layer at the original interface is consistent with the epitaxial thickness concept that predicts defect-free growth for the initial part of the film independent of the growth temperature. The fitted results for surface S values also show that the an-

TABLE II. Summary of fitted results for MBE samples with $T_{\mathrm{growth}} = 220$ °C and $T_{\mathrm{RTA}} = 450$ °C. The symbol, $L_{+,\mathrm{eff}}$ refers to the effective diffusion length of positrons in the defective layer, t_{film} refers to the thickness of the epilayer, and E refers to the constant electric field. The symbols T_m and T_a denote the measurement temperature and the anneal temperature, respectively. A positive electric field indicates a direction into the bulk silicon. c is the defect concentrations in terms of an atomic fraction (at. fr.) for the defective part of the film. The defective part of the film extends from the top surface to a depth of ζ, which is always less than the MBE-grown film thickness.

t_{film} (nm)	T_m (°C)	T_a (°C)	ζ (nm)	$L_{+,\mathrm{eff}}$ (nm)	E (V/cm)	c (at. fr.)
200	20	20	127±9	82±4	8400±1300	2.2×10^{-5}
	200	200	90±8	63±3	0	4.1×10^{-5}
	20	200	120±10	90±5	6100±900	1.8×10^{-5}
	350	350	133±10	90±6	0	1.8×10^{-5}
	20	350	129±10	131±7	1250±170	0.6×10^{-5}
300	20	20	169±6	101±4	900±120	1.3×10^{-5}
	200	200	162±3	113±3	0	9.8×10^{-6}
	20	200	174±6	103±4	1050±140	1.2×10^{-5}
	330	330	201±5	145±5	0	4.1×10^{-6}
	20	330	178±5	115±3	550±100	9.2×10^{-6}

neal at temperatures above 350 °C resulted in permanent changes.

B. Ion scattering and electrical characterization

Even though the positron experiment gives a very large signal for $T_{RTA} = 450\,°C$, indicative of defects in part of the sample, the amount of defects is still very small and in fact unobservable with standard structural techniques. Cross-sectional electron microscopy (TEM) has shown no defects in samples prepared under similar circumstances.[25] The results of ion scattering are illustrated in Fig. 7. There we plot the ratio between backscattered yield in a (100) channeling direction and the yield in random incidence (minimum yield) as a function of T_{RTA}. He^+ with an energy of 2 MeV in normal incidence have been used for the experiment. The backscattered particles, detected with a scattering angle of 175 °, originated from a depth of ≈ 70 nm. To exclude unintentional channeling effects in the random direction, the sample was rotated continuously around its surface normal. The shaded band in Fig. 7 is the minimum yield of a virgin substrate including one standard deviation to each side. Independent of T_{RTA}, all films agree with this control sample, indicating that the sensitivity of ion scattering is insufficient to detect the point defects that have been shown to exist at $T_{RTA} = 450\,°C$ by PAS.

The absence of any evidence for defects in the ion-scattering data is not inconsistent with the defect concentration determined by PAS. From Fig. 7 we conclude that a change of 2×10^{-3} in the minimum yield is statistically significant. That corresponds to 1×10^{20} cm^{-3} displaced atoms, 2 orders of magnitude above the concentration determined by PAS for the film grown with $T_{RTA} = 450\,°C$. Furthermore, ion scattering is most sensitive for displaced atoms, whereas PAS indicates the presence of vacancylike defects.

The dramatic difference in defect concentration between films grown with $T_{RTA} = 450\,°C$ and $T_{RTA} = 600\,°C$ found by PAS has been confirmed qualitatively by electrical measurements on p-n junctions. 150 nm of Si p-doped with B to a concentration of N_B, grown on a p(B) Si(100) substrate doped to 8.5×10^{18} cm^{-3}, was followed by 150 nm of Si n-doped with Sb to a concentration of N_{Sb}. The diode was capped with 20 nm of Si doped with Sb at $N_{Sb,cap}$. After mesaisolation and metallization[6] current-voltage characteristics were recorded at room temperature and are shown in Fig. 8. Two batches of diodes were investigated, both grown at 220 °C, but with different RTA temperatures and slightly different doping concentrations. Their parameters are listed in Table III.

The forward current density of a p-n junction can be written as[26]

$$j_F = j_0 e^{\frac{qV_F}{nkT}}, \tag{6}$$

where V_F is the forward voltage, T the temperature, and j_0, q, and k are a constant, the elementary charge, and Boltzmann's constant, respectively. The factor n is called the "ideality factor": If the carrier transport in the junction is solely due to diffusion, i.e., if there are no electrically active defects of any kind, $n = 1$. If transport is dominated by recombination, i.e., in the presence of a large number of defects, $n = 2$. As can be seen from Fig. 8, the diode of batch 1 with $T_{RTA} = 450\,°C$ has a significantly larger ideality factor than the diode of batch 2 ($T_{RTA} = 600\,°C$). In fact the numerical value of $n = 1.94$ for $T_{RTA} = 450\,°C$ indicates that in this case the forward current is dominated by recombination effects, i.e., the material exhibits a large number of defects. In contrast,

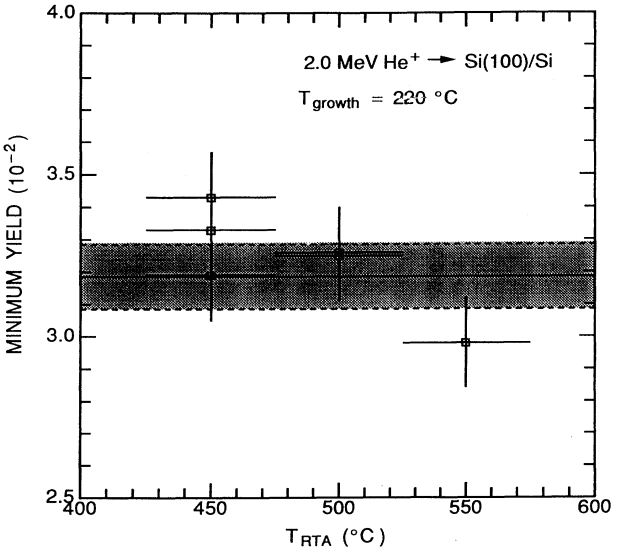

FIG. 7. Minimum yield in normal incidence for 200-nm-thick film grown at 220 °C on Si(100) and annealed every ≈ 30 nm for 2 min to T_{RTA}. 2.0-MeV He^+ ions have been utilized at a scattering angle of 175 °.

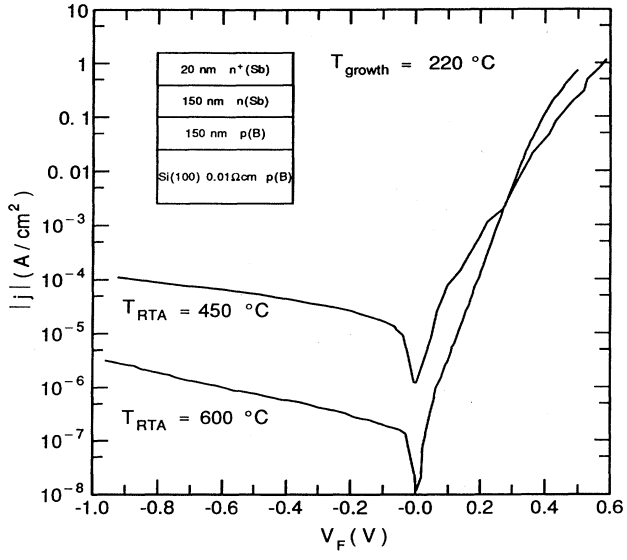

FIG. 8. Absolute value of current density as a function of forward bias for mesa isolated p-n junctions grown at 220 °C by low-temperature MBE with different RTA temperatures. The junction structure is shown schematically in the inset.

TABLE III. Growth parameters of diodes used for the electrical characterization of LT-MBE films. T_{RTA} denotes the RTA temperature, N_B and N_{Sb} the dopant concentration of the p and n side of the junction, respectively, and $N_{Sb,cap}$ the Sb concentration in the cap.

Batch	T_{RTA} (°C)	N_{Sb} ($\times 10^{17}$cm^{-3})	N_B ($\times 10^{17}$cm^{-3})	$N_{Sb,cap}$ ($\times 10^{19}$cm^{-3})
1	450	2.3	4.8	3
2	600	9.4	2.4	15

for $T_{RTA} = 600\,°C$ we obtain the practically perfect value of $n = 1.05$.

In the absence of quantum-mechanical tunneling and at voltages below breakdown of the junction due to an avalanche or thermal effects, the reverse current density can be written as[26]

$$j_R = \frac{qWn_i}{\tau}\,, \tag{7}$$

where W is the width of the junction, n_i the intrinsic carrier concentration, and τ the minority carrier lifetime. Note that Eq. (7) assumes that the doping concentration is sufficiently high for the generation current in the depletion region to dominate. Equation (7) also implies that the reverse current is independent of reverse voltage. As can be seen from Fig. 8, this is not the case for the diode grown at $T_{RTA} = 600\,°C$. Instead the reverse current increases with reverse voltage in an approximately exponential fashion. Such a behavior could in principle be due to electrically active defects; however, the excellent ideality factor argues against this explanation. Alternately, the dependence of the reverse current on reverse voltage could be due to tunneling. As has been discussed elsewhere, LT-MBE allows the growth of very abrupt junctions[6] and, as can be seen from Table III, both sides are fairly highly doped. Estimates of the field at the junction yield values on the order of 3×10^5 V/cm. Band-to-band tunneling is thus indeed expected to play a significant role[26,27] and we ascribe the voltage-dependent increase in reverse current to tunneling. Tunneling should play less of a role in the diodes of batch 1 compared to batch 2, since the former were grown with smaller dopant concentrations than the latter. Despite this, diodes with $T_{RTA} = 450\,°C$ show a significantly *higher* reverse current density than diodes with $T_{RTA} = 600\,°C$. While a quantitative determination of minority carrier lifetimes from the reverse current is not possible without the use of simulations that are beyond the scope of this paper, we can nevertheless conclude that the minority carrier lifetime in the films grown for batch 1 is significantly smaller than for batch 2. This implies again the presence of defects in films with $T_{RTA} = 450\,°C$, as expected from the ideality factors.

C. Defects in films grown by SPE

The S-E results from a sample grown by solid-phase epitaxy are shown in Fig. 9. A comparison to the MBE

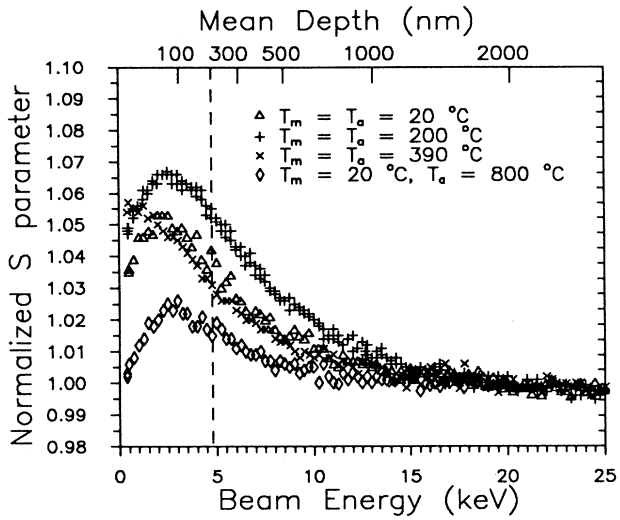

FIG. 9. S parameter vs energy curves for 200 nm Si on Si(100) grown by SPE. The symbols denote: (△) $T_m = T_a = 20\,°C$, (+) $T_m = T_a = 200\,°C$, (×) $T_m = T_a = 390\,°C$, and (◇) $T_m = 20\,°C$, $T_a = 800\,°C$.

results demonstrates that the epitaxial layer grown by SPE is more defective (indicated by the higher S value in the grown film) than a MBE film with $T_{RTA} > 450\,°C$, as observed also by Schut *et al.*[28] A room-temperature measurement of the SPE sample after a 2-h 800 °C vacuum anneal is also included. The fitting gives a defective layer of thickness 71 ± 30 nm and a defect concentration of 2.4×10^{18} cm^{-3} before the 800 °C anneal. After the 800 °C anneal, the defect concentration is reduced to 5.9×10^{17} cm^{-3} with a layer thickness of 105 ± 34 nm. This defective character of the SPE-grown material is consistent with the small electrical activation of dopants in film grown by SPE.[6,29]

V. CONCLUSION

We have demonstrated that thin Si films can be grown by MBE with point-defect concentrations below the sensitivity of PAS, even at growth temperatures as low as 220 °C. Such a low-growth temperature requires, however, periodic rapid thermal anneals to a peak temperature T_{RTA}. The crystalline quality of the film is a sharp function of T_{RTA}: under our experimental conditions (growth rate 0.02 nm/s, duration of RTA pulse 2 min, every 30 nm) $T_{RTA} > 450\,°C$ leads to defect-free material, indistinguishable from the substrate, whereas $T_{RTA} = 450\,°C$ results in vacancylike defects at a concentration $\simeq 10^{18}$ cm^{-3} in the top half (closest to the surface) of the film.

Schut *et al.*[28] have previously investigated MBE films by PAS. They conclude that even at a growth temperature of 730 °C film grown by MBE contain open volume defects at concentrations of the order of 3×10^{18} cm^{-3}. The data presented here show that this is not an inherent property of the MBE growth. Indeed the defects observed in Ref. 28 are probably related to the substrate preparation prior to epitaxial growth: Schut *et al.* point

out that their cleaning technique leads to carbide precipitates. Such precipitates may act as sources of dislocations which could be responsible for the defects observed in Ref. 28. Similarly Perovic *et al.*[30] observed a large positron signal, ascribed to microvoids, in Si films grown at 400 °C at a rate of 0.5 nm/s. The authors note the relatively poor vacuum of 5×10^{-8} torr during growth and the incomplete cleaning of the substrate prior to growth, leading to a very large number of stacking faults and thereby dislocations at the substrate and/or buffer layer interface directly visible to cross-sectional TEM. Furthermore, Perovic *et al.* report their results for film of 6.3-μm thickness. The epitaxial thickness at 400 °C is $\simeq 1$ μm at a rate of 0.07 nm/s, and $\simeq 200$ nm at 5.0 nm/s,[31] i.e., the film in Ref. 30 has exceeded h_{epi} significantly.

The epitaxial thickness at 60 °C is $\simeq 7.0$ nm for a growth rate of 0.02 nm/s, i.e., the first few nm of growth during SPE are crystalline; epitaxy breaks down after this initial region and the remainder of the film is amorphous. As the results in Sec. IV C indicate annealing *in situ* is not sufficient to recover a high-quality, defect-free film, once epitaxy has broken down. We observe vacancylike defects at a concentration of 2.4×10^{18} cm^{-3} after annealing at 550 °C. Even after 2 h at 800 °C defects are still present at a concentration of 5.9×10^{17} cm^{-3}.

In conclusion we have shown that excellent Si films can be grown by MBE at low temperatures when accompanied by an appropriate RTA cycle. We have also illustrated how PAS is a sensitive and useful probe to monitor defect concentrations at a level lower than all other structural techniques, but of direct consequence to the electronic properties of the material.

ACKNOWLEDGMENT

The work at Brookhaven National Laboratory was supported in part by the U.S. Department of Energy under Contract No. DE-AC02-76CH00016. The expert substrate preparation of T. Boone is greatly appreciated.

[1] R.N. Thomas and M.H. Francombe, Solid State Electron. **12**, 799 (1969).
[2] For a review see, for example, H.-J. Gossmann and E.F. Schubert, CRC Crit. Rev. Solid State Mater. Sci. **18**, 1 (1993).
[3] D.J. Eaglesham, H.-J. Gossmann, and M. Cerullo, Phys. Rev. Lett. **65**, 1227 (1990).
[4] H.-J. Gossmann, P. Asoka-Kumar, T.C. Leung, B. Nielsen, K.G. Lynn, F.C. Unterwald, and L.C. Feldman, Appl. Phys. Lett. **61**, 540 (1992).
[5] H.-J. Gossmann, E.F. Schubert, D.J. Eaglesham, and M. Cerullo, Appl. Phys. Lett. **57**, 2440 (1990).
[6] H.-J. Gossmann, F.C. Unterwald, and H.S. Luftman, J. Appl. Phys. **73**, 8237 (1993).
[7] P.J. Schultz and K.G. Lynn, Rev. Mod. Phys. **60**, 701 (1988).
[8] A.P. Mills, Jr. and R. Wilson, Phys. Rev. A **26**, 490 (1982).
[9] See, for example, *Positrons in Solids*, edited by P. Hautojärvi (Springer-Verlag, New York, 1979).
[10] A. van Veen, H. Schut, J. de Vries, R.A. Hakvoort, and M.R. Ypma, in *Positron Beams for Solids and Surfaces*, edited by P.J. Schultz, G.R. Massoumi, and P.J. Simpson, AIP Conf. Proc. No. 218 (American Institute of Physics, New York, 1990), p. 171.
[11] S. Dannefaer, G.W. Dean, D.P. Kerr, and B.G. Hogg, Phys. Rev. B **14**, 2709 (1976).
[12] P. Mascher, S. Dannefaer, and D. Kerr, Phys. Rev. B **40**, 11 764 (1989).
[13] B. Nielsen (unpublished). See also J. Keinonen, M. Hautala, E. Rauhala, V. Karttunen, A. Kuronen, J. Räisänen, J. Lahtinen, A. Vehannen, E. Punkka, and P. Hautojärvi, Phys. Rev. B **37**, 8269 (1988).
[14] A. Ishizaka and Y. Shiraki, J. Electrochem. Soc. **133**, 666 (1986).
[15] M. Tabe, Jpn. J. Appl. Phys. **21**, 534 (1982).
[16] V.M. Donnelly and J.A. McCaulley, J. Vac. Sci. Technol. A **8**, 84 (1990).
[17] M. Tabe, K. Arai, and H. Nakamura, Surf. Sci. **99**, L403 (1980).
[18] E.H. Nicollian and J.R. Brews, *MOS (Metal Oxide Semiconductor) Physics and Technology* (Wiley, New York, 1982), pp. 668 and 711.
[19] G.W. Trucks, K. Raghavachari, G.S. Higashi, and Y.J. Chabal, Phys. Rev. Lett. **65**, 504 (1990).
[20] G.S. Higashi, Y.J. Chabal, G.W. Trucks, and K. Raghavachari, Appl. Phys. Lett. **56**, 656 (1990).
[21] K.G. Lynn, B. Nielsen, and J.H. Quateman, Appl. Phys. Lett. **47**, 239 (1985).
[22] Pulsar 11 Model No. 7000GP, E^{2}T Technology Corp., Ventura, California 93003.
[23] B. Nielsen, K.G. Lynn, Y.C. Chen, and D.O. Welch, Appl. Phys. Lett. **51**, 1022 (1987).
[24] B. Nielsen, K.G. Lynn, A. Vehanen, P.J. Schultz, Phys. Rev. B **32** (1985).
[25] D.J. Eaglesham (private communication).
[26] S.M. Sze, *Physics of Semiconductor Devices* (Wiley, New York, 1981).
[27] A.G. Chynoweth, W.L. Feldman, C.A. Lee, R.A. Logan, G.L. Pearson, and P. Aigrain, Phys. Rev. **118**, 425 (1960).
[28] H. Schut, A. van Veen, G.F.A. van de Walle, and A.A. van Gorkum, J. Appl. Phys., **70**, 3003 (1991).
[29] A. Casel, H. Kibbel, F. Schäffler, Thin Solid Films **183**, 351 (1990).
[30] D.D. Perovic, G.C. Weatherly, P.J. Simpson, P.J. Schultz, T.E. Jackman, G.C. Aers, J.-P. Noël, and D.C. Houghton, Phys. Rev. B **43**, 14257 (1991).
[31] H.-J. Gossmann and D.J. Eaglesham, in *Semiconductor Interfaces, Microstructures, and Devices: Properties and Application*, edited by Z.C. Feng (Institute of Physics, Bristol, 1992).